Numerical phantom generation to evaluate non-rigid CT/CBCT registration algorithms for prostate cancer radiotherapy

Mathieu Rubeaux[1,2], Guillaume Cazoulat[1,2], Aurélien Duménil[1,2], Caroline Lafond[1,2,3], Oscar Acosta[1,2], Renaud de Crevoisier[1,2,3], Antoine Simon[1,2], and Pascal Haigron[1,2]

[1] INSERM, U 1099, Rennes, F-35000, France
[2] Université de Rennes 1, LTSI, F-35000, France
[3] Département de Radiothérapie, Centre Eugène Marquis, Rennes, F-35000, France
mrubeaux@gmail.com

Abstract. In Image-Guided Radiation Therapy of prostate cancer, the CBCT scan acquired at each treatment fraction could be used to estimate a cumulative dose distribution thanks to non-rigid registration. However, this cumulative dose estimation is highly sensitive to non-rigid registration errors. For this reason, validation of the registration algorithm with organ overlap measures or visual assessment is not sufficient. In this paper, we describe the construction of a numerical phantom based on a finite element model of the prostate and the neighbor organs which can be used to assess the non-rigid registration accuracy. Preliminary results show the potential of this phantom to better characterize registration algorithms than traditional Dice score.

1 Introduction

Image-Guided Radiation Therapy (IGRT) aims at increasing the precision of radiation dose delivery. In the context of prostate cancer, a planning Computed Tomography (CT) image with manually defined prostate and organs at risk (OAR) delineations is usually associated with daily Cone Beam Computed Tomography (CBCT) follow-up images. The CBCT images allow to visualize the prostate position and to reposition the patient accordingly. The goal of this rigid registration step is to avoid the prostate being under-irradiated and subsequently the main OARs (bladder and rectum) to be over-irradiated. However, prostate rigid motion is not the only anatomical variation from fraction to fraction. Large deformations can occur due to bladder and rectum filling variations, leading to a received dose that can differ from the planned one. At any fraction, if dose criteria are not met, the clinician may decide to replan the treatment. To compare the actually received dose with the prescribed one, non-rigid registration is used to estimate the tissue deformation to be able to compute the dose locally accumulated.

In order to register pelvic CT and CBCT images, some approaches have been proposed [1, 2], which combine non-rigid registration and segmentation in order to propagate CT delineations in the CBCT images. To evaluate the accuracy of the registration algorithms used in this context, the Dice score remains one widely used criteria, even if it has been shown [3] that it does not necessarily reflect the quality of the registration. Indeed, the Dice score measures the overlap between two delineations, which

in our context are the CBCT delineations and the propagated CT delineations. It only characterizes the correspondance of the organs, whereas it is necessary to evaluate the local matching of the voxels. Indeed, the radiotherapy requires a precise knowledge of the local dose accumulation. However, obtaining a reference of this local matching is very difficult with real images. Another approach is to use the Target Registration Error using pairs of landmarks that are automatically or manually defined. But due to the poor quality of the CBCT images, this is a difficult task, and the landmarks are usually placed on distinctive anatomical marks (e.g bones), where the registration quality is not as crucial as on the considered organs. Recently, new validation approaches have been developed in order to better characterize the quality of registration algorithms [4]. Our work is part of the effort made to bring some new evaluation procedures for CT/CBCT non-rigid registration of pelvic structures.

To do so, a numerical phantom is generated using a biomechanical model integrating the prostate and the OARs (bladder, rectum and seminal vesicles). This phantom is realistic enough to allow non-rigid registration without modifying algorithm parameters that would be used for real subject registration. Moreover, the transformation model used to generate the numerical organs is different from the ones usually used in non-rigid registration, allowing a fair comparison between different kind of algorithms. Even if these deformations remain simple, they give some answers regarding the validity of the deformation fields estimated during registration.

In the first section, the approach used to generate the numerical phantom is described in detail. Then, some non-rigid registration methods under study are explained, justifying the different components of the scheme. Finally, some preliminary results are given, which show that the numerical phantom allows to discriminate more finely between different registration algorithms.

2 Phantom generation

2.1 Biomechanical model

A finite element model of the prostate and OAR (seminal vesicles, bladder, rectum) is used to generate the phantom. It is described using ANSYS DesignModeler. The geometry of the anatomical structures is defined by considering typical sizes and shapes derived from patient CT data. They are represented by parasolid surfaces from either B-splines contours of organs (rectum) or by geometrical sculpting of object (prostate, seminal vesicles, bladder) and then discretized in surface (rectum, bladder) or volume (prostate, seminal vesicles) finite elements.

The simulation is set up by considering typical elastic material properties for the tissues (Young modulus, Poisson ratio) derived from [5, 6]. The organs' wall thickness and the internal pressures for bladder and rectum are obtained from [7]. The values used fo this simulation are provided in table 1. The boundary conditions are defined by fixed supports attached to the extremities of the rectum and the prostate apex, and elastic support to represent organs surrounding the rectum. Moreover contacts are defined between the different organs of interest. The simulation of organ deformations is performed by ANSYS Mechanical. Different values of internal pressure of rectum

Table 1. Linear elastic material properties and Walls thickness

Organ	Poisson's ratio	Young's modulus (kPa)	Wall thickness (mm)
Bladder	0.49	10	2.9
Rectum	0.45	10	2.28
Prostate	0.4	21	
Seminal Vesicles	0.49	10	1

and bladder are applied to deform the structures in a range comparable with typical deformations observed on real patient through CT data.

Typical results of this simulation are given in figure 1. In this preliminary study, two different simulated sets of organs are used: one to generate a CT phantom, the other to create a CBCT phantom.

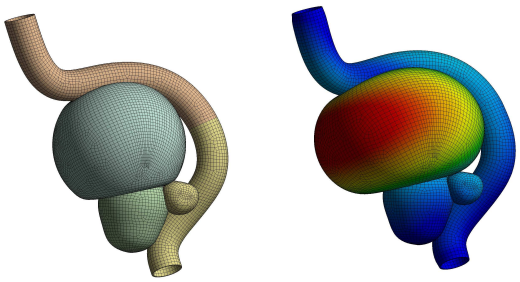

(a) CBCT organs (b) CT organs

Fig. 1. Numerical organs generated using ANSYS. Phantom represented in (a) is used to generate the CBCT phantom, while (b) is used for the CT.

2.2 CT/CBCT reconstruction

To reconstruct synthetic images, the aim is to integrate the finite element models of the different organs in real CT/CBCT images. To do so, two different CT/CBCT images pairs taken from two subjects are considered: the first one ($subjectA$) receive the synthetic organs, while the intensities of the second one ($subjectB$) are used to fill these synthetic organs. The choice to use the organs' intensities of a second subject was guided by technical difficulties encountered while building the phantom. For this data, a clinician manually delineated the prostate and OARs.

The $subjectA$ is drained from its real organs, using the expert delineations. Then the goal is to fill it back with the synthetic organs. The $subjectB$ is used for that purpose. For the bladder and the prostate, an affine registration between the binary images of

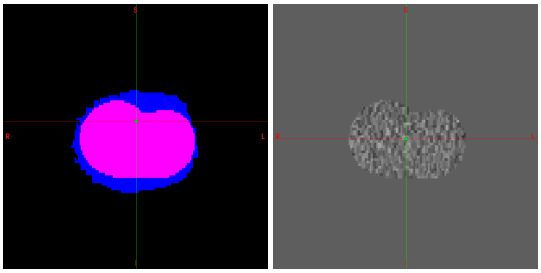

(a) bladder affine registration (b) Filled synthetic bladder

Fig. 2. synthetic CT bladder reconstruction. (a) shows the overlap between syntethic (pink) and $subjectB$ (blue) bladder after affine registration. The intensities of the $subjectB$ bladder taken from the original CT are used to fill the synthetic one (b).

$subjectB$ and the binary images of the synthetic organs is performed. This allows to align the modeled organs with real organs and then to fill the synthetic bladder and prostate with the textures and pixels intensities of $subjectB$.

However, this procedure is not adapted to the rectum and seminal vesicles, due to the geometrical differences between the synthetic organs and the ones of $subjectB$. So some pixels are randomly selected in the $subjectB$ organs to fill the synthetic organs. For the rectum, two regions are differentiated to take into account the gas areas that often come across with the pelvic images. The same procedure is adopted for both CT and CBCT images. An illustration of the synthetic CT bladder reconstruction is given in figure 2.

2.3 Experimental data

Finally, two sets of data are used during the experiments, as shown in figure 3: the numerical CT/CBCT phantom generated as described above, and the $subjectA$, a real patient, which serves as a reference to assess the relevance of the phantom. Two procedures are considered: a phantom CT to CBCT registration, and a real subject CT to CBCT registration.

3 Registration procedure set-up

An iconic registration scheme, taking into account the grey values of the pixels of the images to register, is applied. A registration method is usually defined by i) a similarity measure, ii) a motion model and iii) an optimization procedure. In the experiments, the elastiX toolbox [8] is used during the registration procedures, which allows the reproducibility of the results. The Mutual Information (MI) similarity measure based on Mattes [9, 10] implementation is chosen, since it allows efficient multimodal registration. Regarding the motion model, the registration procedure is divided in two steps: first, a

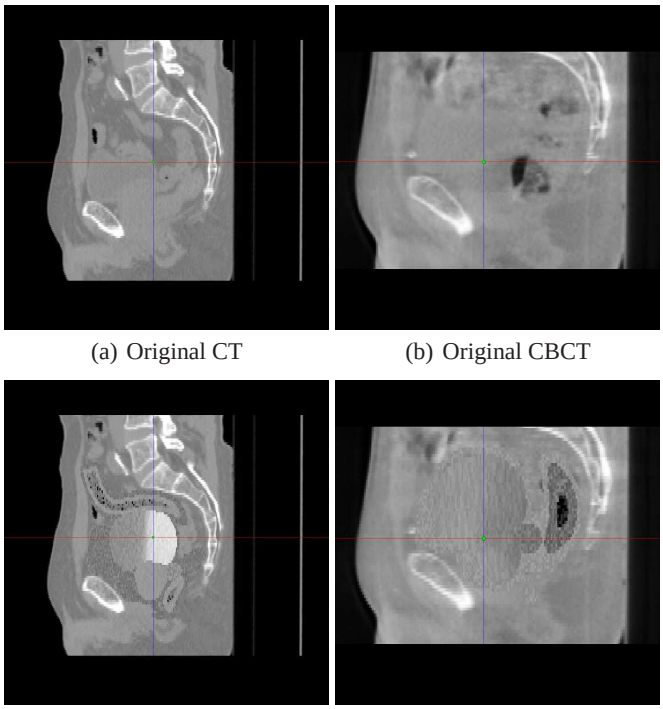

(a) Original CT (b) Original CBCT

(c) Phantom CT (d) Phantom CBCT

Fig. 3. Images used during the tests. (a) Original CT image. (b) Original CBCT image. (c) Generated CT phantom image. (d) Generated CBCT phantom image.

rigid registration to globally align the two images; second, a non-rigid registration using a Free-Form Deformation (FFD) model based on B-Splines [11]. The optimization is based on the adaptive stochastic gradient descent procedure described in [12]. Moreover, a coarse to fine (or pyramidal) approach allows to register global as well as local motion.

Besides this global scheme, the motion is regularized using two different methods: (i) a penalty term based on the bending energy of a thin metal sheet [11], that insures the global smoothness of the transformation.

(ii) a rigid penalty term [13] on the bones that are extracted by thresholding the original image. This term forces the bones to deform rigidly during the non-rigid registration.

In the following, the three methods are compared. MI denotes the registration scheme without regularization, MI_{BE} stands for the registration with a Bending Energy penalty, while MI_{RP} designates the procedure with a Rigid Penalty on the bones.

4 Results

The registration experiments are led using exactly the same parameters for both subject and phantom registration. They are conducted in two steps: first, the Dice scores between the CBCT organs and the propagated CT organs for both phantom and subject registration is calculated. Then, the measures of local estimation errors given by the phantom are provided.

4.1 Dice score

The evaluation of the registration is made using the Dice score to assess the relevance of the phantom compared to the real subject. The results are given in table 2. Two major remarks can be made regarding these results.

First, the Dice scores obtained with the subject and the phantom reach similar levels, even if some differences occur: rectum and seminal vesicles results are slightly better with the phantom, while bladder results seem better on the real subjects. In fact, during the phantom's registration, the drained out organs, which have been refilled with some random pixels taken from fat and muscles of the subject, disturb the registration procedure.

Nevertheless, the results seem promising. Indeed, regarding the different registration algorithms used, one can see that for both datasets, the Dice scores improve when a penalty term is added to the mutual information. On the other hand, by using only the Dice score for validation, it is not possible to choose a particular penalty term, since the results obtained with MI_{BE} and MI_{RP} are relatively close.

Table 2. Dice score obtained for the different organs and registration methods. The results obtained with the phantom are close from those obtained on the subject. The results obtained after the rigid regstration step are also given for comparison.

	Bladder		**Prostate**		**Rectum**		**Seminal Vesicles**	
	Phantom	**Subject**	**Phantom**	**Subject**	**Phantom**	**Subject**	**Phantom**	**Subject**
Rigid	0.70	0.73	0.67	0.76	0.54	0.58	0.34	0.36
MI	0.76	0.79	0.69	0.75	0.60	0.62	0.36	0.37
MI_{BE}	0.79	0.89	0.75	0.83	0.69	0.66	0.63	0.41
MI_{RP}	0.73	0.85	0.91	0.79	0.79	0.66	0.79	0.41

4.2 Local registration errors

The numerical phantom gives access to local validation results that cannot be obtained from the Dice score. Indeed, one can obtain the registration error, as a distance in mm, for each voxel on the surface of the phantom, since we know the exact transformation of the organs between the 2 images. In table 3 are reported the mean, minimum and maximum registration error in mm, for each organ and each registration method. While the

Dice score didn't allow to clearly separate MI_{BE} and MI_{RP} methods, these new error measures are very informative. They show the clear superiority of MI_{RP} compared to MI_{BE} with a total mean error for all the organs which is almost halved (3.76mm for MI_{BE} against 6.09mm for MI_{RP}). They also confirm that taking into account a penalty term during registration improves the results.

Table 3. Local registration errors (in mm), for the different organs and registration methods. This demonstrates the superiority of MI_{RP} compared to MI_{BE}.

		Bladder	**Prostate**	**Rectum**	**SV**
MI	**Mean**	**11.58**	**8.95**	**6.24**	**5.58**
	Min	0.10	0.12	0.08	0.11
	Max	21.42	16.73	15.36	11.22
MI_{BE}	**Mean**	**11.62**	**4.62**	**5.10**	**3.02**
	Min	0.09	0.05	0.06	0.05
	Max	20.32	8.30	12.52	5.16
MI_{RP}	**Mean**	**8.19**	**1.88**	**2.72**	**2.25**
	Min	0.08	0.01	0.02	0.01
	Max	14.94	3.41	6.07	3.06

5 Discussion and conclusion

In this paper, we have presented a numerical phantom of the pelvic structures for CT/CBCT image registration evaluation.

This phantom aims to be a complement to the classical Dice coefficient which do not evaluate the local matching of the organs, on which relies the cumulated dose computation. We showed that this phantom is able to differentiate registration algorithms that cannot be characterized with the use of the Dice score. It especially gives access to a precious information concerning the deformations estimated during registration. Indeed, with its use, the local motion of every voxel on the surface of the phantom can be evaluated precisely.

Regarding the conclusions we can get from the registration evaluation, although the experiments were performed on a reduced data set, it seems that a registration scheme including a rigid penalty term on the bones can produce better results than the traditionnal scheme or the one including a bending energy. This has to be confirmed on a larger dataset, and this will be the object of our future work. The 2 regularization terms given here could also be combined in order to obtain an even better result.

It would also be important to build a phantom which could be closer to a real patient, in order to be able to use affine registration to fill the rectum and seminal vesicles. For that purpose, we plan to generate a patient specific phantom that would take into account the geometrical particularity of each subject.

Acknowledgments

This work was partially funded by the french research agency (ANR): TIGRE project n°ANR-09-BLAN-0378-01.

References

1. Greene, W., Chelikani, S., Purushothaman, K., Knisely, J., Chen, Z., Papademetris, X., Staib, L., Duncan, J.: Constrained non-rigid registration for use in image-guided adaptive radiotherapy. Medical image analysis **13**(5) (2009) 809–817
2. Lu, C., Chelikani, S., Papademetris, X., Knisely, J.P., Milosevic, M.F., Chen, Z., Jaffray, D.A., Staib, L.H., Duncan, J.S.: An integrated approach to segmentation and nonrigid registration for application in image-guided pelvic radiotherapy. Medical Image Analysis **15**(5) (2011) 772–785
3. Rohlfing, T.: Image similarity and tissue overlaps as surrogates for image registration accuracy: Widely used but unreliable. IEEE Transactions on Medical Imaging **31**(2) (2012) 153–163
4. Paganelli, C., Peroni, M., Baroni, G., Riboldi, M.: Validation of deformable registration in adaptive radiation therapy with scale invariant feature transform. In: International Symposium on Biomedical Imaging. (2012)
5. Hensel, J.M., Menard, C., Chung, P.W.M., Milosevic, M.F., Kirilova, A., Moseley, J.L., Haider, M.A., Brock, K.K.: Development of multiorgan finite Element-Based prostate deformation model enabling registration of endorectal coil magnetic resonance imaging for radiotherapy planning. Internationl Journal Radiation Oncology Biology Physics **68**(5) (2007) 1522–1528
6. Chai, X., van Herk, M., van de Kamer, J.B., Hulshof, M.C., Remeijer, P., Lotz, H.T., Bel, A.: Finite element based bladder modeling for image-guided radiotherapy of bladder cancer. Medical physics **38**(1) (January 2011) 142–150
7. Boubaker, M.B., Haboussi, M., Ganghoffer, J.F., Aletti, P.: Finite element simulation of interactions between pelvic organs: Predictive model of the prostate motion in the context of radiotherapy. Journal of Biomechanics **42**(12) (August 2009) 1862–1868
8. Klein, S., Staring, M., Murphy, K., Viergever, M., Pluim, J.: elastix: a toolbox for intensity-based medical image registration. IEEE Transactions on Medical Imaging **29**(1) (2010) 196 – 205
9. Thévenaz, P., Unser, M.: Spline pyramids for inter-modal image registration using mutual information. In: Proceedings of the SPIE Conference on Mathematical Imaging: Wavelet Applications in Signal and Image Processing V. Volume 3169., San Diego CA, USA (1997) 236–247
10. Mattes, D., Haynor, D.R., Vesselle, H., Lewellen, T.K., Eubank, W.: PET-CT image registration in the chest using free-form deformations. IEEE Transactions on Medical Imaging **22**(1) (2003) 120–128
11. Rueckert, D., Sonoda, L., Hayes, C., Hill, D., Leach, M., Hawkes, D.: Nonrigid registration using Free-Form Deformations: Application to breast MR images. IEEE Transactions on Medical Imaging **18**(8) (1999) 712–721
12. Klein, S., Pluim, J., Staring, M., Viergever, M.: Adaptive stochastic gradient descent optimisation for image registration. International Journal of Computer Vision **81**(3) (2009) 227–239
13. Staring, M., Klein, S., Pluim, J.: A Rigidity Penalty Term for Nonrigid Registration. Medical Physics **34**(11) (November 2007) 4098 – 4108